Modeling 3-D Fluid Flow for a MEMS Laminar Proportional Amplifier

M.M. Athavale*, H.Y. Li, and A.J. Przekwas
*CFDRC, 215 Wynn Drive, Huntsville, AL 35805
Voice: (205) 726-4817, Fax: (205) 726-4806, E-mail: mma@cfdrc.com
B.H. Piekarski**, R.J. Zeto, S.M. Tenney
**U.S. Army Research Laboratory, 2800 Powder Mill Rd. Adelphi, MD 20783
Voice: (301) 394-1263, Fax: (301) 394-4562, E-mail: bpiekarski@msc.arl.mil

ABSTRACT

Fluid flow in a microfluidic laminar proportional amplifier (LPA) was simulated using an advanced 3-D flow solver, CFD-ACE+. Pressure gains for single-stage and two-stage blocked output LPAs were calculated under a variety of flow conditions and compared with experimental data. Modeled gains compared well with results from experiments and established design correlations. The accuracy of the results on the complex amplifier flows demonstrates the flow solver's capability to yield reliable predictions and its potential usefulness in the design and performance predictions of microfluidic devices.

Keywords: Flow simulation, fluid dynamics, fluidic amplifier, MEMS processing.

INTRODUCTION

The area of fluidics was initiated in 1959. Subsequent research has produced a variety of fluidic components, including the laminar proportional amplifier (LPA) for amplifying low-level pressure signals [1].

Figure 1 shows the layers necessary to make a six-layer stacked or single-stage LPA. Typically, layers of the stacked LPA are made by etching or machining patterns into stainless steel laminations that are then bolted together. For small-scale LPAs with supply nozzle widths of 250 μm or less, machining techniques are not viable and photochemical milling is the preferred fabrication technique. Photochemical milling does have drawbacks in that it tends to overetch some of the critical design features and forms nonperpendicular sidewalls in the LPA due to undercutting of the photoresist [1]. To minimize this effect, thin laminates of less than 152 μm are used and then stacked to obtain the desired supply nozzle aspect ratios. Even with this technique, accurate features of less than 125 μm are difficult to achieve.

Silicon micromachining techniques have been used to etch single LPA patterns into a silicon wafer with features as small as 6 μm wide and 35 μm deep [2,3]. In these studies, only a single-layer LPA was fabricated and the stage did not include any of the normal venting layers as shown in figure 1. These single amplifier layers were not etched all the way through the wafer and were capped by either a brass or glass input/output manifold to form a functioning single-stage LPA.

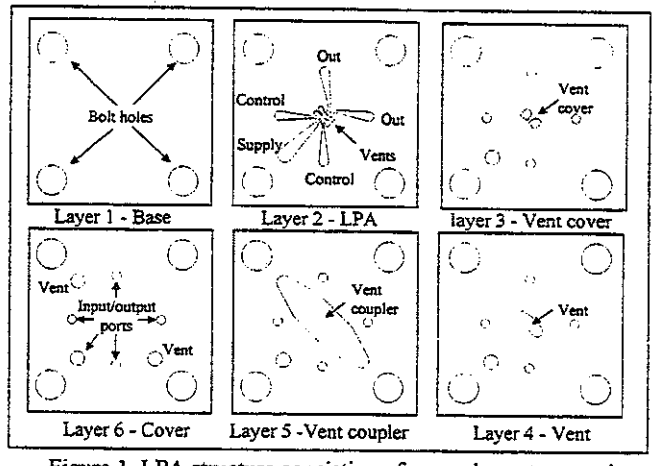

Figure 1. LPA structure consisting of a supply port, control ports, venting ports, and output ports.

Scientists at the U.S. Army Research Laboratory (ARL) are investigating the fabrication of an entire six-layer single-stage LPA in silicon using state-of-the-art microelectromechanical (MEMS) processing technologies (e.g., deep reactive ion etching (DRIE), wafer-to-wafer pattern alignment, and silicon-to-silicon fusion bonding) [4]. DRIE techniques enable etching of features with perpendicular sidewalls completely through the silicon wafer. Precise alignment of features on multiple wafers for building 3-D structures can be accomplished with wafer-to-wafer alignment techniques. Silicon fusion bonding technologies enable an airtight seal between layers. The goal is to improve LPA performance by improving the LPAs fabrication and geometrical conformance to design criteria.

With improved MEMS processing techniques and the ability to accurately fabricate small-scale LPAs, many of the traditional design rules that assume overetching during photochemical milling need to be reevaluated. Flow simulation tools are necessary to efficiently develop these new design rules for optimizing next-generation micromachined LPA devices.

EXPERIMENTAL SETUP

The six-layer, single-stage LPA modeled and experimentally tested for this study is shown in figure 1. Layers 1, 3, 4, 5, and 6 were fabricated in stainless steel by photochemical milling, and each was 254 μm thick. The amplifier layer, layer 2, was fabricated in stainless steel by photochemical milling (76 μm thick) and also fabricated in silicon by DRIE (152 μm thick). To obtain various supply nozzle aspect ratios to test, several layer-2 amplifiers were stacked to get stainless steel and silicon layer-2 amplifiers with effective thicknesses of 152 μm and 304 μm. A third stainless steel amplifier layer with a thickness of 127 μm was fabricated by stacking two stainless steel laminates that were out of thickness tolerance. With these two materials and three thicknesses, five configurations of the single-stage LPA were fabricated and tested. A completely silicon single-stage LPA that uses DRIE for fabricating all six layers, silicon wafer alignment and prebonding tools for wafer-to-wafer pattern alignment, and silicon fusion bonding to fuse the stack together is being fabricated and will be reported on later [4].

Figure 2 shows the location of several critical design features within the amplifier layer, where b_s = nozzle width, b_t = distance between control edges, b_c = control width, b_{sp} = splitter width, b_o = receiver width, x_{sp} = nozzle-to-splitter distance, and x_{th} = nozzle straight channel length [1].

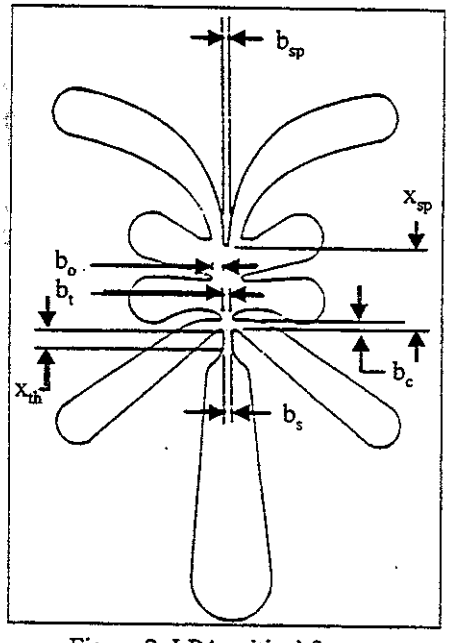

Figure 2. LPA critical features

Table 1 shows some of the critical LPA design dimensions and the deviations that occurred during fabrication of both the stainless steel and preliminary silicon layer-2 amplifier patterns at ARL.

The dimensions and geometrical conformance of the traditional stainless steel LPA varied greatly from the model. In particular, the control width (b_c) and the distance between control edges (b_t). Geometrically, the control edges, vent edges, and jet splitter were pointed instead of having a 63.5-μm radius like the model and silicon amplifier layer. The silicon LPA was in very close tolerance and geometrical conformance to the model. Slight overetching occurred in these initial fabrication runs and is expected to be minimized in subsequent silicon amplifier patterns.

Table 1. LPA dimensions

Design feature	Design (modeled)	Stainless LPA	Silicon LPA
b_s (μm)	124	124-167	126-138
b_c (μm)	127	160-228	125-140
b_t (μm)	142	240-285	144-162
x_{sp} (μm)	1018	1235	1057

Figure 3 shows the basic experimental setup used to measure the single-stage pressure gain for the LPAs (P_s = supply pressure, dP_o = differential output pressure, P_c = control pressure). Figure 4 shows the setup for the two-stage gain measurements. Datametrics barocel pressure sensors of 1000, 100, and 10 Torr were used to measure the supply pressure, differential output pressure, and the control pressure for each test, respectively. Needle valves were used to vary the supply and control pressures and the gain data (dP_o Vs. P_c) was recorded on an Hewlett Packard X-Y recorder.

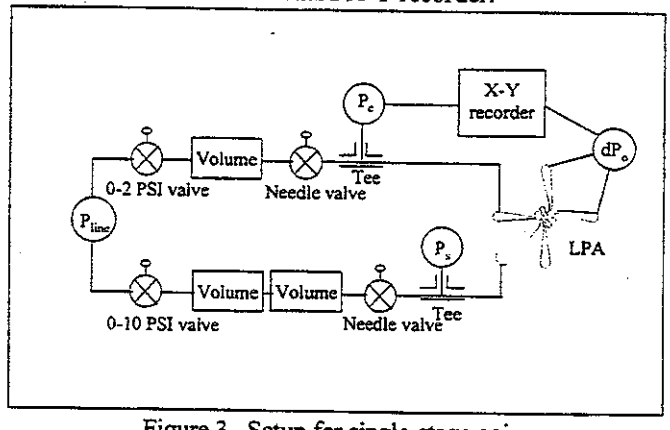

Figure 3. Setup for single-stage gain.

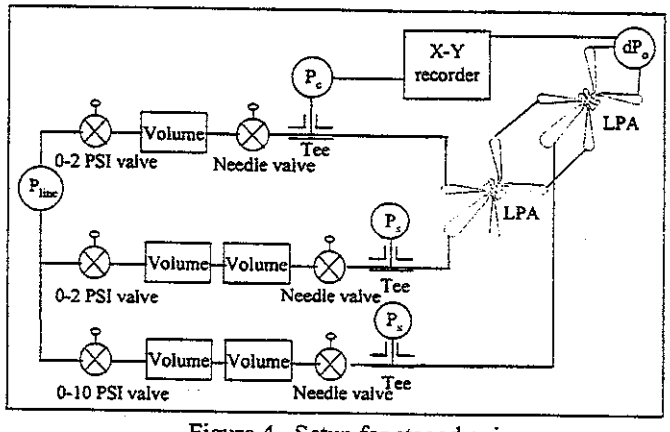

Figure 4. Setup for staged gain.

DESCRIPTION OF THE FLOW SOLVER

Simulations of the LPA were performed using CFD-ACE+ [5], an advanced 3-D Navier-Stokes flow solver that has been adapted to MEMS device simulations [6-8]. The flow domain is discretized and a finite volume method is used to integrate the flow equations. The flow solver uses a pressure-based solution methodology in which the momentum equations are solved sequentially and a pressure Poisson equation, derived from the continuity equation, is solved to correct the pressure and velocities to satisfy the continuity condition. The pressure-based algorithm allows treatment of compressible and incompressible flows. High-order spatial (up to the third order) discretization methods for convection and second-order time discretization methods are available. A number of physical models, including turbulence models, conjugate heat-transfer, and slip-wall conditions for rarified flows are available. A space-conserving moving-grid formulation allows treatment of flows in flow domains with moving-deforming boundaries. Multidisciplinary capabilities including electrostatics, elastostatics, and coupled flow solutions are also available, although not used in the present simulations.

COMPUTATIONAL FLOW DOMAIN

The flow domain of a single-stage LPA consists of the LPA layer, which contains the supply, control, and output channels, and the jet throat area. The central portion of this layer beyond the jet throat is connected to a large vent cavity via a butterfly-shaped, smaller chamber in the central portion of the LPA layer. The flow domain is complicated, and a multidomain grid with five domains and a total of 65 thousand to 90 thousand computational cells was constructed (see fig. 5). The actual device contains a large vent chamber, which

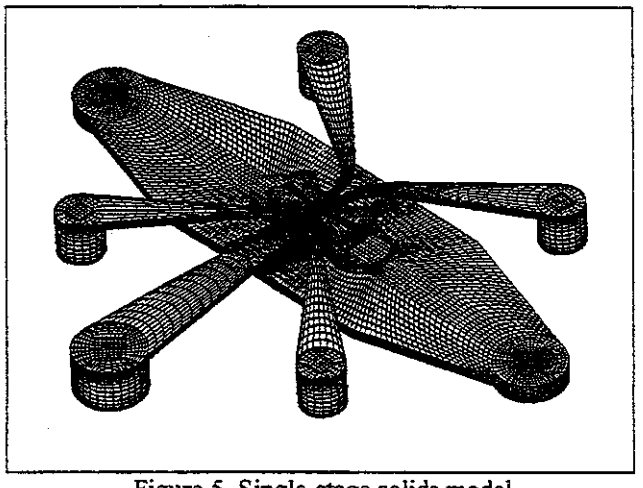

Figure 5. Single-stage solids model.

was modeled exactly during the initial runs. However, to save computational efforts, the chamber was subsequently reduced in size by moving in the vent boundary conditions. Tests were conducted in the original and modified configurations to ensure that the changes in the solutions due to these geometric modifications were insignificant.

BOUNDARY AND FLOW CONDITIONS

Boundary conditions in the single-stage configuration consist of a vent pressure applied to the vent boundary as well as one of the control ports. A supply pressure higher than the vent pressure is applied at the inlet boundary. In the single-stage mode, the two output ports are blocked and the static pressure differential across the two ports is measured. The input signal to the LPA is the control pressure differential, generated by using a pressure level above or below the level of the other control port. All the walls were assumed to be no-slip walls. The vent pressure was held at atmospheric value and air was used as the working fluid. The flow was assumed to be constant property, laminar, and incompressible. Two series of runs were completed in the present study:

1. A Single-stage LPA with blocked output ports (figure 5). The supply pressure was varied from 10 to 40 Torr and the control pressure differential was held fixed at 0.5 Torr. The resulting output pressure differentials were computed and used to calculate the amplifier gain. A few runs at a zero control pressure differential were completed to check the flow symmetry. All three thicknesses of the amplifier layer were considered.

2. Two-stage LPA: Two stages of LPA were cascaded in this series, such that the output ports from the first stage were connected directly to the control ports of the second stage. A solids model of this is shown in figure 6. Such staging of the amplifiers is used to increase gain. High-gain can be obtained

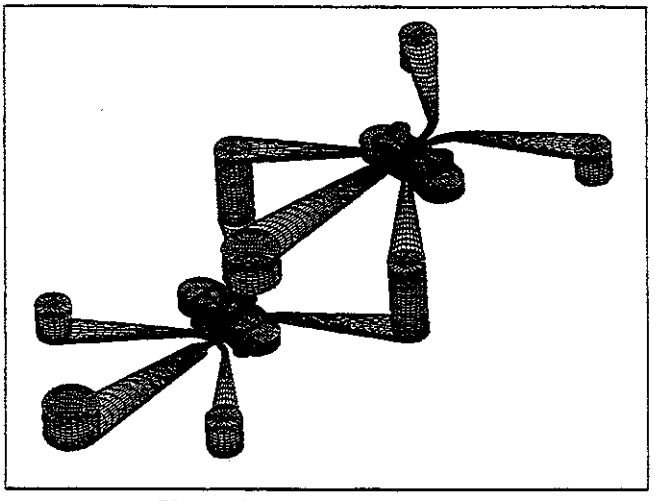

Figure 6. Two-stage solids model.

because individual stage gains are multiplied by each successive stage. Two different configurations were considered in the study: a self-staged LPA where both LPA stages were identical (152-μm thick amplifier layers) and used the same supply pressure of 40 Torr. The second configuration used two different LPA stages with the first using a 304-μm thick amplifier layer and a supply pressure of 10 Torr and the second using a 152-μm thick amplifier layer and a supply pressure of 40 Torr.

RESULTS AND DISCUSSION

Single-stage LPA

The main flow feature in this device is the jet formed at the nozzle that is deflected towards one of the output ports as a result of the control pressure differential. The jet then bifurcates, turns around, and flows down into the vent chamber because the output ports are blocked. The flow eventually exhausts to the vent pressure. A velocity vector plot within the device is shown in figure 7; it clearly shows the jet and its path in the amplifier layer. The corresponding pressure field on the walls is shown in figure 8.

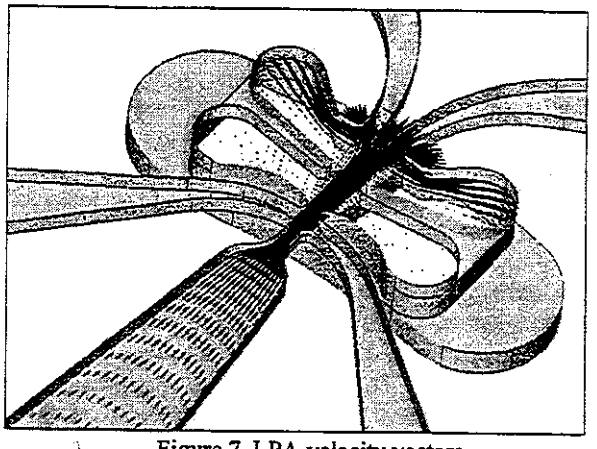

Figure 7. LPA velocity vectors.

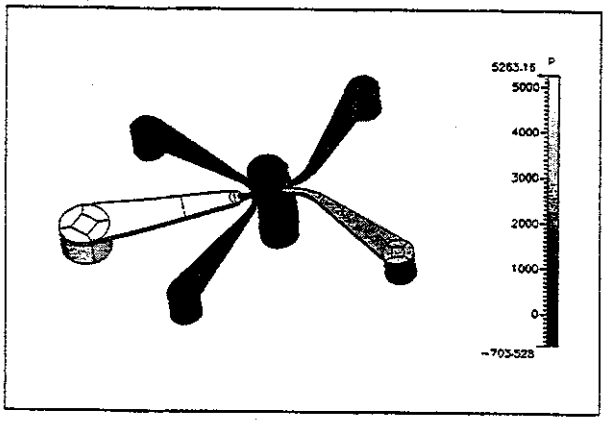

Figure 8. LPA wall pressure distribution.

The gain values of the LPA as a function of the supply pressure were calculated for the 127-μm, 152-μm, and 304-μm thick stainless steel and the 152-μm and 304-μm thick silicon single-stage LPA configurations. Experimental data for these five configurations were generated using the setup described above. Single-stage LPAs with blocked output ports and 127-μm, 152-μm, and 304-μm thick amplifier layers were used in the simulations.

The predicted values of the gain for the 127-μm thick amplifier configuration are shown in figure 9. The predicted values of the gain for the 152-μm thick amplifier configuration are shown in figure 10. Also plotted are the experimental data for comparison. Good correlation between the computed and experimental data was obtained, both in terms of trends and gain values between the model and the experimental data. The gain for the silicon LPA is lower than

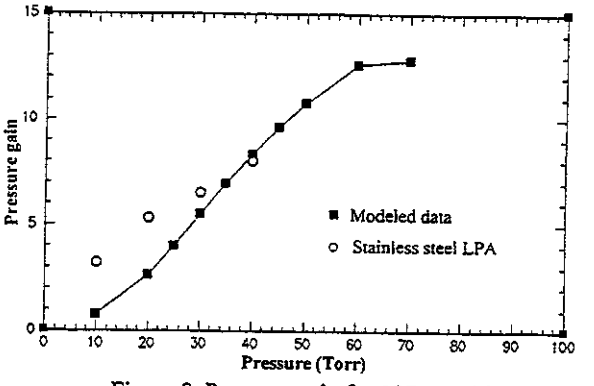

Figure 9. Pressure gain for 127-μm thick single-stage amplifier layer.

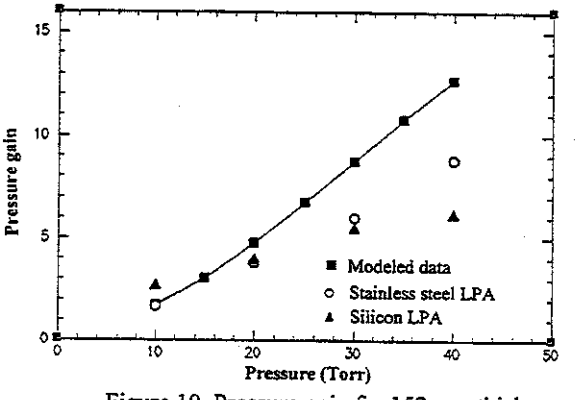

Figure 10. Pressure gain for 152-μm thick single-stage amplifier layer.

both the modeled and stainless steel LPAs at the ideal operating pressure of 40 Torr. Further experimental testing on the silicon LPA indicated a constricted flow condition at the point where the control edges project inward towards the jet. This caused some of the flow to exit through the control ports (in a nonbiased control condition) and reduced the gain by effectively shifting the point where the jet is steered from the nozzle to the control edges. This condition was not present in the stainless steel LPA or the model where flow was actually being evacuated from the control ports when no bias was applied. We hypothesize that the constricted flow was caused in the silicon LPA due to the better conformance to design criteria that moved the control edges much closer together than is typically seen in a traditional stainless steel amplifier layer where the control edges are overetched. We also hypothesize that slight variations in the fabrication of the silicon LPA amplifier led to a more divergent jet than the model. Further modeling is in progress to duplicate the constricted flow condition in the 152-μm configuration. Also, a second iteration of the silicon amplifier layer is being pursued to improve conformance to the design and to slightly alter the design criteria to widen the control edge spacing to eliminate potential constricted flow conditions. We believe

that this will bring the pressure gains closer to those predicted by the model.

The predicted and experimental values of the pressure gain for both 304-μm LPA configurations at a supply pressure of 10 Torr are shown in table 2.

Table 2. LPA Gain

	Model	Stainless	Silicon
Gain	4.76	13	4.5

Good correlation between the computed and experimental data is seen for the model and the silicon LPA. Further experimental testing indicated that a constricted flow condition existed again for the silicon LPA. The model for the 304-μm LPA also showed flow out through the control ports – effectively negative bias – that indicates constricted flow. These results support the hypothesis stated above for the 152-μm configuration. The stainless steel amplifier (with the overetched control edges) did not exhibit the constricted flow condition and had gains close to design guidelines.

A key parameter that controls the LPA performance is the flow Reynolds number (Re) based on the LPA layer thickness and the average jet velocity in the nozzle [1]. Joyce's design calculations [1] use the maximum jet velocity that corresponds to the supply dynamic head. Flow remains laminar below a Re number of about 1000, is transitional between 1000 and 1400, and is turbulent above a Re of 1400. For this reason, LPAs are usually operated below a Re of 1000. A Re based solely on the inlet dynamic head tends to overestimate the values and, hence, the actual calculated mass flux values from the simulations were used to estimate the Re for the two configurations. The variation of modeled gain versus Re is plotted in figure 11 for the 127-μm and 152-μm thick single-stage LPAs. The plot shows that the two sets of results

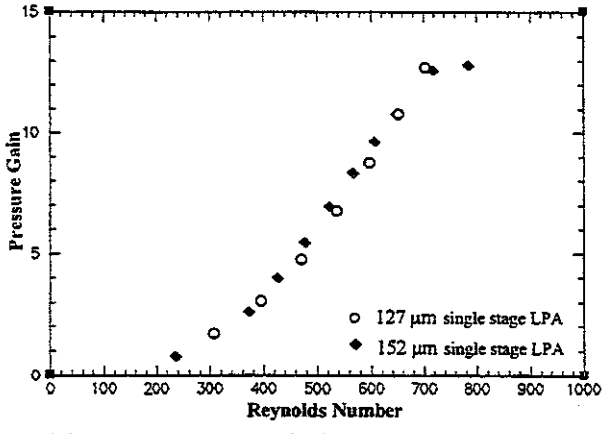

Figure 11. Pressure gain for 127-μm and 152-μm thick amplifier layer

collapse into a single curve that corroborates the guidelines given by Joyce [1] and provides additional proof that the flow physics in the LPA are being predicted accurately by the CFD-ACE+ code. Losses in dynamic head in the supply channel are typically expressed using a coefficient of discharge, C_d, which gives the fraction of inlet dynamic head that was actually converted to jet velocity. A comparison of computed and maximum possible jet velocities indicates that the C_d in the present configurations varies in a narrow range of 0.7 to 0.8, with lower C_d seen at the higher supply pressures.

Staged Amplifiers

Two configurations were analyzed in the present study as described above. In both configurations, first stage control pressure was set at 0.05 Torr. The computed overall gain for the self-staged 152-μm configuration was 70, which was higher than an expected value of approximately 40 [1]. The self-staged nonconstricted stainless steel LPAs had gains of 15-25. These gains were lower than expected and could be attributed to the wider control widths caused by overetching. Wider control widths in the second stage would cause a lower resistance in the output ports of the first stage and lower the overall pressure gain. The silicon two-stage LPA with constricted flow condition for both stages expectedly showed lower staged gains of 10 to 20.

Computations of the second configuration (varying aspect ratio) yielded an overall gain of approximately 49 for the model, which was lower than an expected value of approximately 90. The nonconstricted stainless steel two-stage LPAs had pressure gains of 50 to 90. Variation in the gain data could be attributed to variations in LPA critical dimensions (e.g., control widths). Expectedly, the constricted flow two-stage silicon LPAs had only a limited gain of 17 to 27. Further studies are being performed to investigate the variation of the model from expected values and to fabricate and test nonconstricted staged and self-staged silicon LPAs.

SUMMARY AND CONCLUSIONS

An advanced 3-D CFD code, CFD-ACE+, was successfully used to predict the behavior of fluidic LPAs, both in the single and staged mode. Experiments on single-stage LPAs fabricated in stainless steel and silicon were also conducted and numerical predictions were compared with experimental data.

For a low aspect ratio, 152-μm thick amplifier layer, good agreement between the model and the experimental data was obtained. The silicon LPA had a constricted flow condition resulting in a lower-than-expected gain value due to more faithful pattern definition. Further work is underway to duplicate the constricted flow condition in the model and to modify design criteria to eliminate it from the silicon-fabricated LPA.

Simulations on a high aspect ratio amplifier stage were performed and the results were found to be lower than expected based on design guidelines. Numerical predictions matched the experimental values for the silicon but not the stainless steel LPA. The numerical and experimental analysis

showed a constricted flow condition in both the model and experimental silicon LPA stage. The stainless steel LPA with its overetched control edges did not exhibit constricted flow and had gain values that followed existing design guidelines.

We hypothesize that the modeled design is on the edge of having constricted flow around the control edges and that a slightly more divergent jet in the actual silicon LPA due to slight variations in fabrication could cause the observed constricted flow conditions. Overetching of the control edges in the stainless steel LPA provided enough space to eliminate the constricted flow condition and led to higher gain values than the more faithfully reproduced silicon LPA. This is supported by the numerical analysis that showed expected gain values for the unconstricted flow in the 152-μm thick amplifier layer and lower-than-expected gains for the constricted flow in the 304-μm thick amplifier layer. Further numerical analysis is being performed to validate this hypothesis on a modified 152-μm thick amplifier layer design, where the control edges are moved in to create the constricted flow condition. Also, a second iteration of the silicon amplifier layer with modified design rules is in progress to eliminate potential constricted flow conditions

Simulations were also performed on staged LPAs where two stages were connected in series to increase the overall gain values. The model predicted higher than expected pressure gains for the self-staged configuration and lower than expected gains for the staged configuration. The silicon LPAs could not be directly compared to the model because in all cases, stages were exhibiting constricted flow resulting in lower than expected gain values. Further studies are being performed to investigate the variation of the model and from expected values and to fabricate and test nonconstricted staged and self-staged silicon LPAs.

This study demonstrates the capability of the CFD-ACE+ code to correctly predict the flow phenomena in complex MEMS fluidic devices and produce reliable results. Such predictive capability will be of considerable importance in the design stages of MEMS to prove viability of the devices and aid in device optimization before fabrication.

ACKNOWLEDGEMENTS

The work on simulations was supported by DARPA Contract No. MDA972-97-C-0013 , with Dr. Daniel J. Radack as the Program Monitor. This support is greatly appreciated.

The authors would also like to thank Eugene Zakar, Richard Piekarz and John Conrad from the U.S. Army Research Laboratory for their help in fabricating the silicon LPA structures and test fixtures.

REFERENCES

1. James W. Joyce, "Design Guide for Fluidic Laminar Proportional Amplifiers and Laminar Jet Angular Rate Sensors," Harry Diamond Laboratories, HDL-SR-84-6, 1984.
2. M.J. Zdeblick, P.P. Barth, and J.B. Angel, "A Microminiature Fluidic Amplifier," *Sensors and Actuators*, **15**, 1988, 427-433.
3. Rogerio Furlan and Jay Zemel, "Comparison of Wall Attachment and Jet Deflection Microfluidic Amplifiers," *IEEE Proceedings of Ninth International Workshop on Micro Elecromechanical Systems*, 1996.
4. B.H. Piekarski, R.J. Zeto, and S.M. Tenney, "Fabrication and Testing of a Multilayer Silicon Fusion Bonded Fluidic Laminar Proportional Amplifier," To be presented at *Applications of Micro-Fabrication to Fluid Mechanics* 1998 International Mechanical Engineering Congress and Exposition, Anaheim, CA, November 1998.
5. *CFD-ACE+ User's Manual*, CFD Research Corp., 1997.
6. M.M. Athavale, and A.J. Przekwas, "High-Fidelity CFD Simulations of Microfluidic Devices," *Solid-State Sensors and Actuators Workshop*, Hilton Head, SC, June 1996.
7. A.J. Przekwas, M.M. Athavale, and H.Q. Yang, "A High-Fidelity Simulation Environment for Thermo-Fluid-Mechanical Design of MEMS," Final Report, DARPA contract DAAH01-96-C-R1030, August 1996.
8. M.M. Athavale, H.Q. Yang, and A.J. Przekwas, "Coupled Fluid-Thermo-Structures Simulation Methodology for MEMS Applications, " *TRANSDUCERS-97*, Chicago, IL, June 1997.